Theory for superconductivity in alkali chromium arsenides $A_2Cr_3As_3$ (A=K,Rb,Cs)

Yi Zhou,[1,2] Chao Cao,[3] and Fu-Chun Zhang[1,2]

[1]*Department of Physics, Zhejiang University, Hangzhou 310027, China*
[2]*Collaborative Innovation Center of Advanced Microstructures, Nanjing 210093, China*
[3]*Department of Physics, Hangzhou Normal University, Hangzhou 310036, China*

(Dated: March 3, 2015)

We propose an extended Hubbard model with three molecular orbitals on a hexagonal lattice with D_{3h} symmetry to study recently discovered superconductivity in $A_2Cr_3As_3$ (A=K,Rb,Cs). Effective pairing interactions from paramagnon fluctuations are derived within the random phase approximation, and are found to be most attractive in spin triplet channels. At small Hubbard U and moderate Hund's coupling, the pairing arises from 3-dimensional (3D) γ band and has a spatial symmetry $f_{y(3x^2-y^2)}$, which gives line nodes in the gap function. At large U, a fully gapped p-wave state, $p_z\hat{z}$ dominates at the quasi-1D α-band.

PACS numbers: 74.20.-z; 74.20.Mn; 74.20.Rp; 74.70.-b

Recently, CrAs based superconductors have attracted much attention. CrAs itself is a 3D antiferromagnet (AFM), which becomes superconducting (SC) under modest pressure with $T_c \sim 2$K[1]. Subsequently, a new family of quasi-1D superconductors $A_2Cr_3As_3$ (A=K,Rb,Cs) has been discovered at ambient pressure with T_c up to 6.1K[2–4]. The key building block of $A_2Cr_3As_3$ is the 1D $[(Cr_3As_3)^{2-}]_\infty$ double-walled sub-nanotubes (Fig. 1), which are separated by columns of K^+ ions, in contrast to the layered iron-pnictide and copper-oxide high Tc superconductors.

This new family exhibits interesting properties in both the normal and SC states. In the normal state, the resistivity follows $\rho(T) = \rho_0 + AT$ in a wide temperature region, different from the usual Fermi liquid behavior $\rho_0 + AT^2$[2–4]. NMR measurements on $K_2Cr_3As_3$ showed a power-law temperature dependence $1/T_1 \sim T^{0.75}$ above T_c, which is neither $1/T_1 \sim T$ for a Fermi liquid nor Curie-Weiss behavior $1/T_1T \sim C/(T+\theta)$ for an AFM[5]. Below T_c, the electronic contribution to the specific heat $C_e(T)$ deviates from the BCS senario, and the extrapolated upper critical field H_{c2} exceeds the Pauli limit[2–4]. The Hebel-Slichter coherence peak of $1/T_1$ is absent in $K_2Cr_3As_3$ NMR measurement[5]. London penetration depth measurement for $K_2Cr_3As_3$ shows linear temperature dependence, $\Delta\lambda(T) \sim T$, at temperatures $T \ll T_c$[6]. All these experiments are very difficult to explain within electron-phonon coupling mechanism, and suggest unconventional nature of superconductivity.

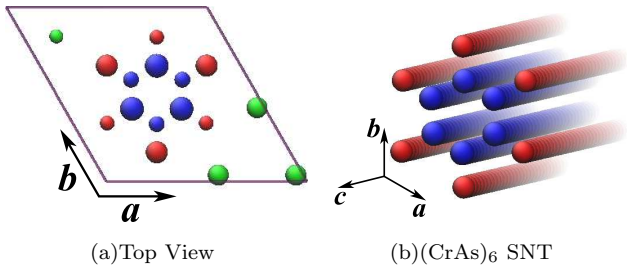

(a)Top View (b)$(CrAs)_6$ SNT

FIG. 1: Crystal structure of $A_2Cr_3As_3$. (a) Top view and (b) the $(Cr_6As_6)_\infty$ sub-nanotube. In panel (a), larger and smaller atoms are at z=0.5 and z=0.0, respectively. In both panels, green balls indicate alkaline atoms, red balls arsenic atoms, and blue balls chromium atoms.

The electronic structure of $K_2Cr_3As_3$ has been investigated by Jiang *et al.*[7] using density functional theory (DFT), which is confirmed by later calculation[8]. There are three energy bands at the Fermi level: two quasi-1D α- and β-bands with flat Fermi surfaces, and a 3D γ-band. It is natural to ask the question, which band is responsible for the superconductivity? On one hand, the linear temperature dependent resistivity and the power-law $1/T_1$ in NMR indicate a quasi-1D Tomonaga-Luttinger liquid; on the other hand, upper critical field measurement H_{c2} implies a 3D superconductor[9]. In this Letter, we shall carry out theoretical study to address this issue. We shall focus on $K_2Cr_3As_3$ and the theory may be extended to other alkali chromium arsenides.

We begin with constructing the Hamiltonian by using symmetries. The space group for $A_2Cr_3As_3$ lattices is $P\bar{6}m2$ and the corresponding point group is D_{3h}.[2–4] We shall also assume that the time reversal symmetry remains unbroken, and consider a system described by the Hamiltonian

$$H = H_0 + H_{int},$$

where H_0 is the non-interacting part and H_{int} is the interacting Hamiltonian.

Tight-binding model. We assume H_0 to be given by a tight-binding Hamiltonian. For $K_2Cr_3As_3$, there are three Fermi surfaces corresponding to the α, β and γ bands. Minimally, we need three orbitals per unit cell (per Cr_6As_6 cluster). From the DFT calculation, there are three low energy molecular orbitals. Two of them belong to 2D irreducible representation E' of D_{3h} group, and the other one is in 1D representation A_1'. We denote two E' states as $|1\rangle$ and $|2\rangle$ and the A_1' state as $|3\rangle$.

Neglecting spin-orbit coupling, the tight-binding Hamiltonian H_0 can be constructed from these three orbitals,

$$H_0 = \sum_{\mathbf{k}mns} c^\dagger_{\mathbf{k}ms}\xi_{\mathbf{k}mn}c_{\mathbf{k}ns}, \quad (1)$$

where $m, n = 1, 2, 3$ are the three molecular orbitals, $s = \uparrow, \downarrow$ is the spin index, $c^\dagger_{\mathbf{k}ms}(c_{\mathbf{k}ms})$ creates an m-orbital electron with spin s. In the basis $\{|1\rangle, |2\rangle, |3\rangle\}$, $\xi_{\mathbf{k}mn}$ can be written in terms of matrix form

$$\hat{\xi}_{\mathbf{k}} = \sum_{\tau=0}^{8} \xi^\tau_{\mathbf{k}}\lambda_\tau, \quad (2)$$

where λ_{1-8} are Gell-Mann matrices.

We now use the symmetry to analyse $\xi^\tau_{\mathbf{k}}, \tau = 1, \cdots, 8$. λ_{1-8} transfer as irreducible representations under D_{3h} symmetry operations. Namely, λ_0 and λ_8 transfer as A_1', λ_2 transfers as A_2', (λ_1, λ_3), (λ_4, λ_6) and (λ_5, λ_7) transfer as E' respectively. H_0 should be invariant under all the D_{3h} symmetry operations, thereby belongs to representation A_1'. Therefore, $\xi^\tau_{\mathbf{k}}$ can be determined using the Clebsch-Gordan coefficients.[10] Since the ab-plane lattice constant $a = 9.98$Å is much larger than that along the c-axis $c = 4.23$Å, we will only keep the hopping terms on ab-plane up to the first nearest neighbor (NN) bonds and those along c-axis up to the second NN bonds. To do this, we set the Bravais lattice basis $\mathbf{a} = (\frac{a}{2}, -\frac{\sqrt{3}a}{2}, 0), \mathbf{b} = (\frac{a}{2}, \frac{\sqrt{3}a}{2}, 0), \mathbf{c} = (0, 0, c)$ (see Fig.1), and introduce $k_a = \mathbf{k}\cdot\mathbf{a}, k_b = \mathbf{k}\cdot\mathbf{b}, k_c = \mathbf{k}\cdot\mathbf{c}$, and some harmonic functions on the ab plane,

$$\begin{aligned} s_{x^2+y^2}(\mathbf{k}) &= \cos k_a + \cos k_b + \cos(k_a + k_b), \\ p_x(\mathbf{k}) &= 2\sin(k_a + k_b) + \sin k_a + \sin k_b, \\ p_y(\mathbf{k}) &= \sqrt{3}(\sin k_b - \sin k_a), \\ d_{x^2-y^2}(\mathbf{k}) &= \cos k_a + \cos k_b - 2\cos(k_a + k_b), \\ d_{xy}(\mathbf{k}) &= -\sqrt{3}(\cos k_b - \cos k_a). \end{aligned} \quad (3)$$

It is easy to verify that $s_{x^2+y^2} \propto 1 - \frac{1}{4}(k_x^2 + k_y^2)$, $p_x \propto k_x$, $p_y \propto k_y$, $d_{x^2-y^2} \propto k_x^2 - k_y^2$ and $d_{xy} \propto k_x k_y$ at small ka. Thus, we have $\xi^2_{\mathbf{k}} = \xi^5_{\mathbf{k}} = \xi^7_{\mathbf{k}} = 0$, and other nonzero $\xi^\tau_{\mathbf{k}}$'s,

$$\begin{aligned} \xi^0_{\mathbf{k}} &= 2t_1\cos k_c + 2t_4\cos 2k_c + 2t_2 s_{x^2+y^2}(\mathbf{k}), \\ \xi^8_{\mathbf{k}} &= 2t_1'\cos k_c + 2t_4'\cos 2k_c + 2t_2' s_{x^2+y^2}(\mathbf{k}), \\ \xi^1_{\mathbf{k}} &= -Ap_y(\mathbf{k}) - Bd_{xy}(\mathbf{k}), \\ \xi^3_{\mathbf{k}} &= Ap_x(\mathbf{k}) - Bd_{x^2-y^2}(\mathbf{k}), \\ \xi^4_{\mathbf{k}} &= Cp_x(\mathbf{k}) - Dd_{x^2-y^2}(\mathbf{k}), \\ \xi^6_{\mathbf{k}} &= Cp_y(\mathbf{k}) + Dd_{xy}(\mathbf{k}), \end{aligned} \quad (4)$$

where $A = (t_3 + t_5\cos k_c), B = (\tilde{t}_3 + \tilde{t}_5\cos k_c), C = (t_3' + t_5'\cos k_c), D = (\tilde{t}_3' + \tilde{t}_5'\cos k_c)$. By fitting the DFT band structure of $K_2Cr_3As_3$, we obtain a set of parameters (in eV) as following: $t_1 = 0.2274$, $t_4 = -0.0573$, $t_2 = -0.0040$, $t_1' = -0.0481$, $t_4' = 0.0242$, $t_2' = 0.0057$, $t_3 = 0.0147$, $t_5 = -0.0023$, $\tilde{t}_3 = 0.0022$, $\tilde{t}_5 = -0.0124$, $t_3' = 0.0015$, $t_5' = -0.0058$, $\tilde{t}_3' = -0.0020$, $\tilde{t}_5' = -0.0297$. We also obtain the chemical potential $\mu_{chem} = 0.2365$ eV. As shown in Fig. 2, the set of parameters well reproduces the Fermi surfaces. They also reproduce the energy dispersion along high symmetry lines and the density of states (DOS) near the Fermi level well[11].

FIG. 2: Comparison of the Fermi surfaces for $K_2Cr_3As_3$ obtained from the DFT calculation (a), and from the present model Hamiltonian (b). The α, β and γ bands are labelled. The Γ point is at the center of the Brillouin zone.

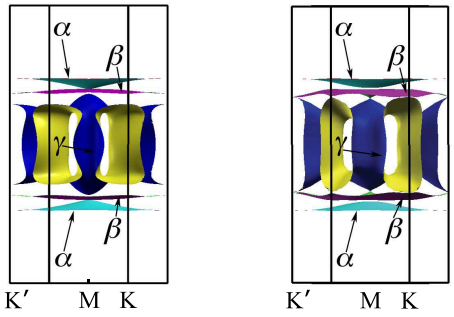

(a) (b)

By diagonalizing H_0 we obtain three energy bands with dispersion $\epsilon_{\mathbf{k}\mu}$ and eigen-wavefunctions $\phi^m_{\mathbf{k}\mu}$, hereafter μ is the band index. The bare susceptibility tensor $\hat{\chi}_0(\mathbf{q})$ is defined as

$$\begin{aligned} \chi_0^{mn,m'n'}(\mathbf{q}) &= -\frac{1}{N}\sum_{\mathbf{k}}\sum_{\mu\nu} \frac{\phi^m_{\mathbf{k}\mu}\phi^{m'*}_{\mathbf{k}\mu}\phi^{m'}_{\mathbf{k}+\mathbf{q}\nu}\phi^{m*}_{\mathbf{k}+\mathbf{q}\nu}}{\epsilon_{\mathbf{k}\mu} - \epsilon_{\mathbf{k}+\mathbf{q}\nu}} \\ &\quad \times [f(\epsilon_{\mathbf{k}\mu}) - f(\epsilon_{\mathbf{k}+\mathbf{q}\nu})], \end{aligned} \quad (5)$$

where $f(\epsilon_{\mathbf{k}\mu})$ is the Fermion occupation number, N is the number of unit cells. Note that $\hat{\chi}_0(\mathbf{q})$ can be also written as a 9×9 matrix in the two-body orbital space spanned by the basis $\{|m\rangle \otimes |n\rangle : m, n = 1, 2, 3\}$.

Interaction: Now we consider the electron-electron interaction. In the spirit of Hubbard approximation, i.e. retaining only the intra-unit-cell terms, we obtain the interacting Hamiltonian which respects D_{3h} symmetry,[11]

$$H_{int} = \frac{1}{2}\sum_i \Big\{ \sum_{m=1}^{2}\sum_{\sigma}[U_1 c^\dagger_{im\sigma}c^\dagger_{im\bar{\sigma}}c_{im\bar{\sigma}}c_{im\sigma} + Jc^\dagger_{im\sigma}c^\dagger_{im\bar{\sigma}}c_{i\bar{m}\bar{\sigma}}c_{i\bar{m}\sigma} + J'(c^\dagger_{im\sigma}c^\dagger_{im\bar{\sigma}}c_{i3\bar{\sigma}}c_{i3\sigma} + h.c.)]$$
$$+ \sum_{m=1}^{2}\sum_{\sigma\sigma'}(U_2 c^\dagger_{im\sigma}c^\dagger_{i\bar{m}\sigma'}c_{i\bar{m}\sigma'}c_{im\sigma} + Jc^\dagger_{im\sigma}c^\dagger_{i\bar{m}\sigma'}c_{im\sigma'}c_{i\bar{m}\sigma} + U_2' c^\dagger_{im\sigma}c^\dagger_{i3\sigma'}c_{i3\sigma'}c_{im\sigma} + J'c^\dagger_{im\sigma}c^\dagger_{i3\sigma'}c_{im\sigma'}c_{i3\sigma})$$
$$+ \sum_{\sigma} U_1' c^\dagger_{i3\sigma}c^\dagger_{i3\bar{\sigma}}c_{i3\bar{\sigma}}c_{i3\sigma}\Big\}, \quad (6)$$

where $\bar{m}$ is the opposite orbital to m within E' representation ($\bar{1}=2$ and $\bar{2}=1$), and $\bar{\sigma}$ is the opposite spin to σ. Here U_1, U_2 and J are intra-orbital repulsion, inter-orbital repulsion and Hund's coupling for the two E' states, which satisfy that $U_1 = U_2 + 2J$. U_1' is the intra-orbital repulsion for the A_1' state, and J' involves one of E' states and the A_1' state.

By Fourier transformation, we have

$$H_{int} = \frac{1}{2}\sum_{\mathbf{k}\mathbf{k}'\mathbf{q}}\sum_{mnm'n'}\sum_{\sigma\sigma'}\Gamma_0^{mn,m'n'}(\mathbf{k},\mathbf{k}-\mathbf{q};\mathbf{k}',\mathbf{k}'+\mathbf{q}) \times c^\dagger_{\mathbf{k}m\sigma}c^\dagger_{\mathbf{k}'m'\sigma'}c_{\mathbf{k}'+\mathbf{q}n'\sigma'}c_{\mathbf{k}-\mathbf{q}n\sigma}, \quad (7)$$

where the bare vertex function $\Gamma_0^{mn,m'n'}(\mathbf{k},\mathbf{k}-\mathbf{q};\mathbf{k}',\mathbf{k}'+\mathbf{q})$ can be written as a matrix in the two-body orbital space,

$$\hat{\Gamma}_0(\mathbf{k},\mathbf{k}-\mathbf{q};\mathbf{k}',\mathbf{k}'+\mathbf{q}) = (1-\delta_{\sigma\sigma'})\hat{\Gamma}_s + \delta_{\sigma\sigma'}\hat{\Gamma}_t, \quad (8)$$

where $\hat{\Gamma}_t$ is bare vetex in the equal-spin channel and $\hat{\Gamma}_s$ is in the opposite-spin channel. The two-body orbital space can be decomposited to subspaces $\{|11\rangle, |22\rangle, |33\rangle\} \oplus \{|12\rangle, |21\rangle\} \oplus \{|13\rangle, |13\rangle\} \oplus \{|23\rangle, |32\rangle\}$. Thus, $\hat{\Gamma}_s$ and $\hat{\Gamma}_t$ are block diagonal in this set of basis,

$$\hat{\Gamma}_s = \begin{pmatrix} U_1 & U_2 & U_2' \\ U_2 & U_1 & U_2' \\ U_2' & U_2' & U_1' \end{pmatrix} \oplus J\Pi \oplus J'\Pi \oplus J'\Pi, \quad (9a)$$

$$\hat{\Gamma}_t = \begin{pmatrix} 0 & U_2 & U_2' \\ U_2 & 0 & U_2' \\ U_2' & U_2' & 0 \end{pmatrix} \oplus J\sigma_1 \oplus J'\sigma_1 \oplus J'\sigma_1, \quad (9b)$$

where σ_1 is Pauli matrix and $\Pi = 1+\sigma_1$ is a 2×2 matrix.

Effective pairing interaction. For weak coupling, the full vertex function $\Gamma^{mn,m'n'}_{\sigma\sigma'}(\mathbf{k},\mathbf{k}-\mathbf{q};\mathbf{k}',\mathbf{k}'+\mathbf{q})$ can be evaluated diagrammatically, for instance, through the random phase approximation (RPA). To study the SC pairing, we only need to keep the vertices in pairing channels with $\mathbf{k}' = -\mathbf{k}$, say, $\hat{\Gamma}_{\sigma\sigma'}(\mathbf{k},\mathbf{k}';-\mathbf{k},-\mathbf{k}') \equiv \hat{V}_{\sigma\bar{\sigma}}(\mathbf{k},\mathbf{k}')$. Therefore, $\hat{V}_{\sigma\sigma}(\mathbf{k},\mathbf{k}') = (1-\delta_{\sigma\sigma'})\hat{V}_s(\mathbf{k},\mathbf{k}') + \delta_{\sigma\sigma'}\hat{V}_t(\mathbf{k},\mathbf{k}')$ serves as an effective pairing interaction to study superconductivity instability.

In study of the cuprates, Scalapino et al. used RPA to calculate $\hat{V}_{\sigma\sigma}(\mathbf{k},\mathbf{k}')$ in a single Hubbard model.[12] The RPA involves two types of Feynman diagrams in addition to the bare vertex function $\hat{V}_0(\mathbf{k},\mathbf{k}')$[11]. One contains the bubble diagrams, and the other contains the ladder diagrams with Cooperon. Here we generalize the calculation in Ref.[12] to the multi-orbital case. The effective pairing interaction $\hat{V}_{s(t)}(\mathbf{k},\mathbf{k}')$ from the bubble diagrams is

$$\hat{V}^{bub}_{s(t)}(\mathbf{k},\mathbf{k}') = \frac{1}{2}\Big\{(\hat{\Gamma}_t+\hat{\Gamma}_s)[1+\hat{\chi}_0(\mathbf{q})(\hat{\Gamma}_t+\hat{\Gamma}_s)]^{-1} \mp(\hat{\Gamma}_t-\hat{\Gamma}_s)[1+\hat{\chi}_0(\mathbf{q})(\hat{\Gamma}_t-\hat{\Gamma}_s)]^{-1}\Big\} \quad (10)$$

where $\mp$ takes $-$ for s and $+$ for t. The effective pairing from the ladder diagrams is

$$\check{V}^{lad}_{s(t)}(\mathbf{k},\mathbf{k}') = \check{\Gamma}_{s(t)}\hat{\chi}_0(\mathbf{p})\check{\Gamma}_{s(t)}[1-\hat{\chi}_0(\mathbf{p})\check{\Gamma}_{s(t)}]^{-1}, \quad (11)$$

where $\mathbf{p} = \mathbf{k}+\mathbf{k}'$ and $\mathbf{q} = \mathbf{k}-\mathbf{k}'$[11]. For the notation, matrix $\check{A}$ is related to matrix $\hat{A}$ via the following relation,

$$\check{A}_{mn,m'n'} = \hat{A}_{nn',mm'}.$$

We can also project effective pairing potential $\hat{V}_{\sigma\sigma'}(\mathbf{k},\mathbf{k}')$ into three single particle bands through

$$V^{\mu\nu}_{\sigma\sigma'}(\mathbf{k},\mathbf{k}') = \sum_{mnm'n'}\phi^{m*}_{\mathbf{k}\mu}\phi^{m'*}_{-\mathbf{k}\mu}V^{mn,m'n'}_{\sigma\sigma'}(\mathbf{k},\mathbf{k}')\phi^{n}_{\mathbf{k}'\nu}\phi^{n'}_{-\mathbf{k}'\nu}, \quad (12)$$

where $\phi^m_{\mathbf{k}\mu}$ is the single particle eigenwavefunction in the μ-band.

Superconducting pairing instability. Because the three Fermi surfaces have different shapes, $\mathbf{k}$ and $-\mathbf{k}$ are always in the same band for $\mathbf{k}$ near the Fermi surfaces. For weak coupling, we only consider intra-band pairing ($\mathbf{k}$ to $-\mathbf{k}$). A single band gap function can be written as

$$\Delta(\mathbf{k}) = i[\sigma_0\psi(\mathbf{k}) + \sigma\cdot\mathbf{d}(\mathbf{k})]\sigma_2, \quad (13)$$

where $\psi(\mathbf{k}) = \psi(-\mathbf{k})$ is the spin-singlet gap function, and the d-vector $\mathbf{d}(\mathbf{k}) = -\mathbf{d}(-\mathbf{k})$ describes the spin-triplet pairing, σ_0 is the unit matrix, $\sigma_{1,2,3}$ are Pauli matrice. To measure the intra-band SC pairing instability, we follow Scalapino *et al.*,[12] and introduce a dimensionless coupling constant

$$\Lambda_\mu = -\frac{\int\frac{dS_{\mathbf{k}\mu}}{|\mathbf{v}_{\mathbf{k}\mu}|}\int\frac{dS_{\mathbf{k}'\mu}}{|\mathbf{v}_{\mathbf{k}'\mu}|}\sum_{\sigma\sigma'}g^\mu_{\sigma\sigma'}(\mathbf{k})^*V^{\mu\mu}_{\sigma\sigma'}(\mathbf{k},\mathbf{k}')g^\mu_{\sigma\sigma'}(\mathbf{k}')}{(2\pi)^3\int\frac{dS_{\mathbf{k}\mu}}{|\mathbf{v}_{\mathbf{k}\mu}|}\sum_{\sigma\sigma'}|g^\mu_{\sigma\sigma'}(\mathbf{k})|^2},$$

where $\int dS_{\mathbf{k}\mu}$ is the integration over the μ-band Fermi surface and $\mathbf{v}_{\mathbf{k}\mu}$ is the Fermi velocity, the μ-band form factor $g^{\mu}_{\sigma\sigma'}(\mathbf{k}) \propto \Delta_{\sigma\sigma'}(\mathbf{k})$.

In the absence of the spin-orbit coupling, the spin-singlet component $\psi(\mathbf{k})$ will not mix with the spin-triplet component $\mathbf{d}(\mathbf{k})$ in Eq.(13). The possible single-band SC gap functions on hexagonal lattice are listed in Table I up to the first and second NN bonds[13].

TABLE I: Superconducting gap functions $\psi(\mathbf{k})$ and $\mathbf{d}(\mathbf{k})$ on hexagonal lattice. The gap functions are intra-band and are classified according to D_{3h} group irreducible representation Γ. The functions $s_{x^2+y^2}$, p_x, p_y, $d_{x^2-y^2}$, and d_{xy} have been defined in Eq.(3). Other functions are defined as follows, $p_z = \sin k_c$, $d_{z^2} = \cos k_c$, $f_{x(x^2-3y^2)} = \sin k_a + \sin k_b - \sin(k_a + k_b)$, $f_{y(3x^2-y^2)} = \sin(2k_a + k_b) - \sin(k_a + 2k_b) - \sin(k_a - k_b)$.

Γ	spin-singlet $\psi(\mathbf{k})$	spin-triplet $\mathbf{d}(\mathbf{k})$
A_1'	$1, s_{x^2+y^2}, d_{z^2}$	$f_{y(3x^2-y^2)}\hat{z}$
A_2'		$f_{x(x^2-3y^2)}\hat{z}$
E'	$(d_{x^2-y^2}, d_{xy})$	$(p_x, p_y)\hat{z}, p_z(\hat{x}, \hat{y})$
A_1''	$p_z f_{y(3x^2-y^2)}$	$p_x\hat{x} + p_y\hat{y}, p_z\hat{z}$
A_2''	$p_z f_{x(x^2-3y^2)}$	$p_y\hat{x} - p_x\hat{y}$
E''	$p_z(p_x, p_y)$	$(p_x\hat{x} - p_y\hat{y}, p_y\hat{x} + p_x\hat{y})$

We next examine all the pairing states in Table I to investigate which pairing channel will dominate. For simplicity, we set $U_1 = U_1' = U$, $U_2' = U_2$ and $J' = J$ at first. The relevant Λ_μ's are plotted as functions of J/U in Fig. 3, and those Λ_μ not plotted have either negative or negligibly small values.

Fig. 3(a) shows the pair coupling constant in various channels for $U = 0.5$ eV. Results for $U < 0.5$eV are similar. The spin-triplet $f_{y(3x^2-y^2)}$ state in the γ-band appears at a finite J/U and become dominant when $J/U > 1/3$. The $f_{y(3x^2-y^2)}$ state has a line nodal gap. Fig. 3(c) plots the results at $U = 2$ eV, to represent large U. In that case, the spin-triplet $p_z\hat{z}$ state at the α-band dominates in all the realistic region of $J/U < 0.45$. The $p_z\hat{z}$ state has a full gap at the quasi-1D α-band Fermi surface. In the intermediate region, e.g., $U = 1.0$eV, $p_z\hat{z}$ and $f_{y(3x^2-y^2)}$ state compete against each other, $p_z\hat{z}$ dominates at small J/U, while $f_{y(3x^2-y^2)}$ state become strong at large J/U. We have also calculated the pair coupling constant for $J' \neq J$ while keep $U_1 = U_1' = U$ and $U_2' = U_2$. The results are similar in a wide parameter region $0.5 < J'/J < 2.0$. Note that at large U and J/U, the SC pairing is found in the β-band with pairing symmetry $p_x\hat{x} \pm p_y\hat{y}$ and $p_y\hat{x} \pm p_x\hat{y}$, which gives point nodal in the gap function. However, Λ_μ for these point nodally gapped states are tiny.

Note that the divation of our tight-binding model from DFT results in some details would not change the above statements qualitatively. Because it is the Fermi surface shape and DOS near the Fermi level that determine Λ_μ and pairing symmetry in weak coupling.

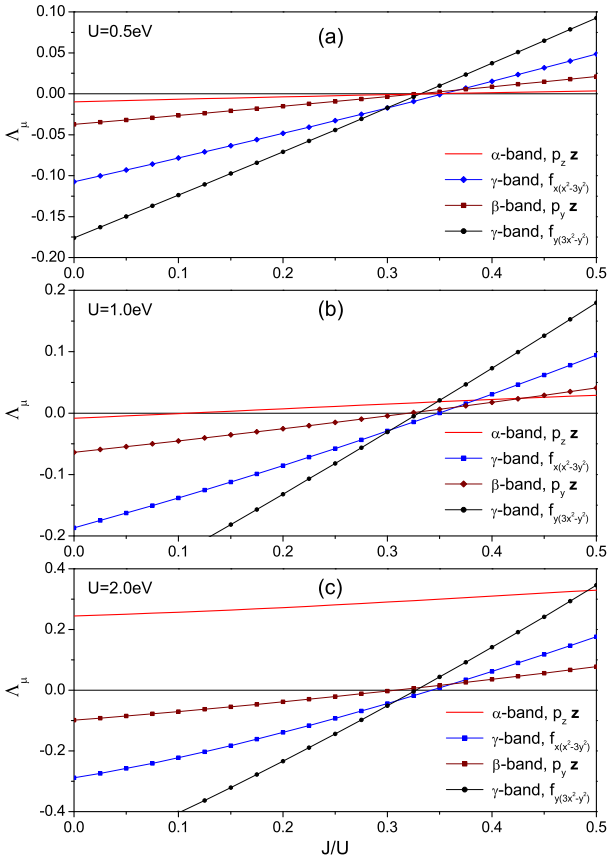

FIG. 3: The dimensionless pair coupling constant Λ_μ vs J/U for (a) $U = 0.5$eV, (b) $U = 1.0$eV and (c) $U = 2.0$eV. Here we have set $U_1 = U_1' = U$, $U_2' = U_2$ and $J' = J$. All the dominated states are spin-triplet pairing states. (a) $U = 0.5$eV, $f_{y(3x^2-y^2)}$ appear and dominate when $J/U > 1/3$. (b) $U = 1.0$eV, $p_z\hat{z}$ state and $f_{y(3x^2-y^2)}$ compete against each other. (c) $U = 2.0$eV, $p_z\hat{z}$ state dominates over most J/U.

Discussions and Summary We would like to mention some issues which have not been addressed in this paper but may be interesting for future work. (i) We neglect spin-orbit coupling in the theory for simplicity. Actually the D_{3h} lattice breaks inversion symmetry, and the spin-orbit coupling may mix spin singlet and triplet states within the same D_{3h} irreducible representation in Table I. (ii) We have only considered intra-unit-cell interaction in the Hubbard model. Since the Wannier functions are extended in a Cr_6As_6 cluster, the inter-unit-cell interaction along the c-axis could be sizable. (iii) Since molecular orbitals are more extended than atomic orbitals, U and J are estimated to be smaller than or comparable to the bandwidth. In this paper we start with weak coupling to study SC instability. However, $A_2Cr_3As_3$ lattice is quasi-1D, an alternative approach would be to model the system as a coupled Tomonaga-Luttinger liquid.

In summary, we have proposed a minimal model to study superconductivity in $A_2Cr_3As_3$ (A=K,Rb,Cs), which involves three molecular orbital states in each unit

cell. With the help of symmetry, we have deduced a tight-binding model with 3 molecular orbitals for the system, which compares well with the results of the density functional theory. We have derived effective pairing interactions within the RPA, and found that the dominant pairing channel is always spin-triplet. For small U, a spin-triplet state with line nodal gap, $f_{y(3x^2-y^2)}$, at the 3D γ-band will dominate at moderate Hund's coupling. While for large U, a spin-triplet fully gapped state, $p_z\hat{z}$, will dominate at the quasi-1D α-band. The state we find at small U appears to be most relevant to the compound. The pairing state of $f_{y(3x^2-y^2)}$ has nodal lines on planes $k_a = k_b$, $k_a = -2k_b$ and $k_b = -2k_a$, say, Γ-K-L-A planes on hexagonal lattices. The Γ-K-L-A planes cross small sections at γ-Fermi surface. Our theory at small U predicts line zeroes in gap function and appears to be consistent with existing experiments showing non-BCS gap function and particularly the low temperature London penetration depth measurement. Our prediction can be tested in further experiments including angle resolved photoemission spectroscopy.

Acknowledgment We would like to thank G.H. Cao, Z.A Xu, H.Q. Yuan, F.L. Ning, J. Zhao and H. Yao and D. F. Agterberg for helpful discussions. This work is supported in part by National Basic Research Program of China (No.2011CBA00103/2014CB921201/2014CB921203), NSFC (No.11374256/11274269/11274006), NSF of Zhejiang Province (No. LR12A04003).

[1] W. Wu, J. Cheng, K. Matsubayashi, P. Kong, F. Lin, C. Jin, N. Wang, Y. Uwatoko, and J. Luo, Nat. Commun. 5, 5508 (2014).
[2] Jin-Ke Bao, Ji-Yong Liu, Cong-Wei Ma, Zhi-Hao Meng, Zhang-Tu Tang, Yun-Lei Sun, Hui-Fei Zhai, Hao Jiang, Hua Bai, Chun-Mu Feng, Zhu-An Xu, Guang-Han Cao, Phys. Rev. X 5, 011013 (2015).
[3] Zhang-Tu Tang, Jin-Ke Bao, Yi Liu, Yun-Lei Sun, Abduweli Ablimit, Hui-Fei Zhai, Hao Jiang, Chun-Mu Feng, Zhu-An Xu, Guang-Han Cao, Phys. Rev. B 91, 020506(R) (2015).
[4] Zhang-Tu Tang, Jin-Ke Bao, Zhen Wang, Hua Bai, Hao Jiang, Yi Liu, Hui-Fei Zhai, Chun-Mu Feng, Zhu-An Xu, Guang-Han Cao, Science China Materials, 58(1), 16-10 (2015).
[5] H. Z. Zhi, T. Imai, F. L. Ning, Jin-Ke Bao, Guang-Han Cao, eprint arXiv:1501.00713 (2015)
[6] G. M. Pang, M. Smidman, W. B. Jiang, J. K. Bao, Z. F. Weng, Y. F. Wang, L. Jiao, J. L. Zhang, G. H. Cao, H. Q. Yuan, eprint arXiv:1501.01880 (2015).
[7] Hao Jiang, Guanghan Cao, Chao Cao, eprint arXiv:1412.1309 (2014).
[8] Xianxin Wu, Congcong Le, Jing Yuan, Heng Fan, Jiangping Hu, eprint arXiv:1501.00412 (2015).
[9] Tai Kong, Sergey L. Bud'ko, Paul C. Canfield, eprint arXiv:1501.01554 (2015).
[10] P. H. Butler, Point Group Symmetry Applications: Methods and Tables, Plenum Press, New York (1981).
[11] See supplementary materials for details.
[12] D. J. Scalapino, E. Loh, Jr., and J. E. Hirsch, Phys. Rev. B 35, 6694 (1987).
[13] We thank Daniel F. Agterberg for pointing out the correct $\hat{x}, \hat{y}, \hat{z}$ transformation under horizontal reflection σ_h, who found a similar table as Table I.

Supplementary Material: Theory for superconductivity in alkali chromium arsenides $A_2Cr_3As_3$ (A=K,Rb,Cs)

D_{3h} GROUP: CHARACTER TABLE, CLEBSCH-GORDAN COEFFICIENTS AND OTHERS

In this section, we provide useful informations on the point group D_{3h}, which have been used to determine the formatoin of Hamiltonian and analyze superconducting pairing symmetry.

Character table

D_{3h} group is a direct product of D_{3h} group and a Z_2 group generated by the horizontal reflection σ_h, namely, $D_{3h} = D_3 \otimes \sigma_h$. The character table for D_{3h} is the following.

Below we list some functions for D_{3h} irreducible representations on hexagonal lattice, limited to the second NN bonds.

TABLE II: Character table for D_{3h} group.

$D_{3h}=D_3\times\sigma_h(\bar{6}m2)$			E	$2C_3$	$3C_2$	σ_h	$2S_3$	$3\sigma_v$
x^2+y^2,z^2	$x(x^2-3y^2)$	A_1'	1	1	1	1	1	1
	$y(3x^2-y^2)$	A_2'	1	1	-1	1	1	-1
(x^2-y^2,xy)	$(x,y),(xz^2,yz^2)$	E'	2	-1	0	2	-1	0
$yz(3x^2-y^2)$		A_1''	1	1	1	-1	-1	-1
$xz(x^2-3y^2)$	z,z^3	A_2''	1	1	-1	-1	-1	1
(xz,yz)	$(z(x^2-y^2),zxy)$	E''	2	-1	0	-2	1	0

TABLE III: Functions for D_{3h} group representation on hexagonal lattice.

$D_{3h}=D_3\times\sigma_h(\bar{6}m2)$		
$\cos(k_a+k_b)+\cos k_a+\cos k_b$	$\sin k_a+\sin k_b-\sin(k_a+k_b)$	A_1'
	$\sin(2k_a+k_b)-\sin(k_a+2k_b)-\sin(k_a-k_b)$	A_2'
$(\cos k_a+\cos k_b-2\cos(k_a+k_b),\sqrt{3}(\cos k_b-\cos k_a))$	$(2\sin(k_a+k_b)+\sin k_a+\sin k_b,\sqrt{3}(\sin k_b-\sin k_a))$	E'
		A_1''
	$\sin k_c$	A_2''
$\sin k_c(\cos k_a+\cos k_b-2\cos(k_a+k_b),\sqrt{3}(\cos k_b-\cos k_a))$	$\sin k_c(2\sin(k_a+k_b)+\sin k_a+\sin k_b,\sqrt{3}(\sin k_b-\sin k_a))$	E''

Since

$$\begin{aligned} k_a &= \frac{1}{2}k_x-\frac{\sqrt{3}}{2}k_y,\\ k_b &= \frac{1}{2}k_x+\frac{\sqrt{3}}{2}k_y, \end{aligned}$$

when $ka\ll 1$, we have

$$\begin{aligned} \cos k_a+\cos k_b-2\cos(k_a+k_b) &\simeq \frac{3}{4}(k_x^2-k_y^2),\\ \sqrt{3}(\cos k_b-\cos k_a) &\simeq -\frac{3}{2}k_xk_y,\\ 2\sin(k_a+k_b)+\sin k_a+\sin k_b &\simeq 3k_x,\\ \sqrt{3}(\sin k_b-\sin k_a) &\simeq 3k_y. \end{aligned}$$

Clebsch-Gordan coefficients

We shall also find out Clebsch-Gordan (CG) coefficients for later use. Since $D_{3h}=D_3\otimes\sigma_h$, we only need to consider the CG coefficents for D_3 group. For D_3 group, there are three representations A_1, A_2 and E, where A_1 and A_2 are 1D and E is 2D. The natural notations for A_1 and A_2 are 0 and $\tilde{0}$ respectively, say, $|0\rangle$ and $|\tilde{0}\rangle$ denote A_1 and A_2 states respectively. We also denote the two E states as $|1\rangle$ and $|-1\rangle$. Here $|1\rangle$ and $|-1\rangle$ are two eigenstates whose eigenvalue under C_3 rotation are $e^{i\frac{2\pi}{3}}$ and $e^{-i\frac{2\pi}{3}}$ respectively. The two E states can be also written as $|x\rangle$ and $|y\rangle$, which are related to $|\pm1\rangle$ as

$$|\pm1\rangle=\frac{1}{\sqrt{2}}(|x\rangle\pm i\,|y\rangle).$$

For the decomposition $\Gamma_1\otimes\Gamma_2=\oplus\Gamma$, we have

$$\begin{aligned} |0\rangle &= |0,0\rangle=|\tilde{0},\tilde{0}\rangle=\frac{1}{\sqrt{2}}\left(|1,-1\rangle+|-1,1\rangle\right),\\ |\tilde{0}\rangle &= |0,\tilde{0}\rangle=|\tilde{0},0\rangle=\frac{1}{\sqrt{2}}\left(|1,-1\rangle-|-1,1\rangle\right),\\ |1\rangle &= |0,1\rangle=|1,0\rangle=|\tilde{0},1\rangle=|1,\tilde{0}\rangle=|-1,-1\rangle,\\ |-1\rangle &= |0,-1\rangle=|-1,0\rangle=-|\tilde{0},-1\rangle=-|-1,\tilde{0}\rangle=|1,1\rangle. \end{aligned}$$

In terms of $|x\rangle$ and $|y\rangle$, we also have

$$\begin{aligned}
|0\rangle &= \frac{1}{\sqrt{2}}\left(|x,x\rangle + |y,y\rangle\right), \\
\left|\tilde{0}\right\rangle &= \frac{1}{\sqrt{2}i}\left(|x,y\rangle - |y,x\rangle\right), \\
|x\rangle &= |0,x\rangle = |x,0\rangle = \left|\tilde{0},x\right\rangle = \left|x,\tilde{0}\right\rangle = \frac{1}{\sqrt{2}}(|x,x\rangle - |y,y\rangle), \\
|y\rangle &= |0,y\rangle = |y,0\rangle = \left|\tilde{0},y\right\rangle = \left|y,\tilde{0}\right\rangle = \frac{-1}{\sqrt{2}}(|x,y\rangle + |y,x\rangle).
\end{aligned}$$

The CG coefficients for D_3 group can be extended to D_{3h} group straightforward, via the following correspondence between D_{3h} irreducible representations and D_3 irreducible representations,

$$\begin{aligned}
A_1'' &= \sigma_h A_1' \leftrightarrow A_1, \\
A_2'' &= \sigma_h A_2' \leftrightarrow A_2, \\
E'' &= \sigma_h E' \leftrightarrow E.
\end{aligned}$$

How $\hat{x}, \hat{y}, \hat{z}$ transfer under σ_h

To analyze the spin-triplet pairing states, one need to study how the basis $\hat{x}, \hat{y}, \hat{z}$ transfer under D_{3h} symmetry operations, especially under the operation σ_h. The basis states $\hat{x}, \hat{y}, \hat{z}$ are defined as

$$\begin{aligned}
\hat{x} &= \left|S_x^{tot} = 0\right\rangle = \frac{1}{\sqrt{2}}\left(-|\uparrow\uparrow\rangle + |\downarrow\downarrow\rangle\right), \\
\hat{y} &= \left|S_y^{tot} = 0\right\rangle = \frac{1}{\sqrt{2}}\left(|\uparrow\uparrow\rangle + |\downarrow\downarrow\rangle\right), \\
\hat{z} &= \left|S_z^{tot} = 0\right\rangle = \frac{1}{\sqrt{2}}\left(|\uparrow\downarrow\rangle + |\downarrow\uparrow\rangle\right).
\end{aligned}$$

Note that the horizontal reflection can be written as

$$\sigma_h = IC_{2z} = I\exp(-\frac{i\pi}{2}\sigma_z) = -iI\sigma_z,$$

where I is the inversion operation. Since angular momentum operators and their eigenstates will not change under I, we have

$$\begin{aligned}
\sigma_h\left|\uparrow\right\rangle &= -i\left|\uparrow\right\rangle, \\
\sigma_h\left|\downarrow\right\rangle &= i\left|\downarrow\right\rangle.
\end{aligned}$$

Therefore

$$\begin{aligned}
\sigma_h\hat{x} &= \frac{1}{\sqrt{2}}\sigma_h\left(-|\uparrow\uparrow\rangle + |\downarrow\downarrow\rangle\right) = -\hat{x}, \\
\sigma_h\hat{y} &= \frac{1}{\sqrt{2}}\sigma_h\left(|\uparrow\uparrow\rangle + |\downarrow\downarrow\rangle\right) = -\hat{y}, \\
\sigma_h\hat{z} &= \frac{1}{\sqrt{2}}\sigma_h\left(|\uparrow\downarrow\rangle + |\downarrow\uparrow\rangle\right) = \hat{z}.
\end{aligned}$$

We would like to thank Daniel F. Agterberg for pointing out this correct transformation, who found a similar table as Table I in the main text.

DERIVATION OF H_0 AND COMPARISON WITH DFT CALCULATION

A generic three-orbital tightbinding model without spin-orbit coupling can be written as

$$H_0 = \sum_{\mathbf{k}mns} c^\dagger_{\mathbf{k}ms}\xi_{\mathbf{k}mn}c_{\mathbf{k}ns}.$$

In the basis $\{|1\rangle, |2\rangle, |3\rangle\}$, the Hermitian matrix $\hat{\xi}_{\mathbf{k}}$ can be expressed in terms of Gell-Mann matrices,

$$\hat{\xi}_{\mathbf{k}} = \sum_{\tau=0}^{8} \xi_{\mathbf{k}}^{\tau} \lambda_{\tau},$$

where GellMann matrices λ_{1-8} are defined with the unit matrix λ_0 as follows,

$$\begin{aligned}
\lambda_0 &= \begin{pmatrix} 1 & 0 & 0 \\ 0 & 1 & 0 \\ 0 & 0 & 1 \end{pmatrix}, \lambda_1 = \begin{pmatrix} 0 & 1 & 0 \\ 1 & 0 & 0 \\ 0 & 0 & 0 \end{pmatrix}, \lambda_2 = \begin{pmatrix} 0 & -i & 0 \\ i & 0 & 0 \\ 0 & 0 & 0 \end{pmatrix}, \\
\lambda_3 &= \begin{pmatrix} 1 & 0 & 0 \\ 0 & -1 & 0 \\ 0 & 0 & 0 \end{pmatrix}, \lambda_4 = \begin{pmatrix} 0 & 0 & 1 \\ 0 & 0 & 0 \\ 1 & 0 & 0 \end{pmatrix}, \lambda_5 = \begin{pmatrix} 0 & 0 & -i \\ 0 & 0 & 0 \\ i & 0 & 0 \end{pmatrix}, \\
\lambda_6 &= \begin{pmatrix} 0 & 0 & 0 \\ 0 & 0 & 1 \\ 0 & 1 & 0 \end{pmatrix}, \lambda_7 = \begin{pmatrix} 0 & 0 & 0 \\ 0 & 0 & -i \\ 0 & i & 0 \end{pmatrix}, \lambda_8 = \sqrt{\frac{1}{3}} \begin{pmatrix} 1 & 0 & 0 \\ 0 & 1 & 0 \\ 0 & 0 & -2 \end{pmatrix}.
\end{aligned}$$

The issue is how to determine $\xi_{\mathbf{k}}^{\tau}$. Writing $\varphi_{\mathbf{k}s}^{\dagger} = (c_{\mathbf{k}1s}^{\dagger}, c_{\mathbf{k}2s}^{\dagger}, c_{\mathbf{k}3s}^{\dagger})$, then we can find out how $\varphi_{\mathbf{k}s}^{\dagger} \lambda_{\tau} \varphi_{\mathbf{k}s}$ transfer under D_{3h} symmetry operations. From the CG coefficients, we find that they can be classified to different irreducible representations of D_{3h} group.

$$\begin{aligned}
A_1' &: \varphi_{\mathbf{k}s}^{\dagger} \lambda_0 \varphi_{\mathbf{k}s}, \varphi_{\mathbf{k}s}^{\dagger} \lambda_3 \varphi_{\mathbf{k}s} \\
A_2' &: \varphi_{\mathbf{k}s}^{\dagger} \lambda_2 \varphi_{\mathbf{k}s}, \\
E' &: (\varphi_{\mathbf{k}s}^{\dagger} \lambda_1 \varphi_{\mathbf{k}s}, \varphi_{\mathbf{k}s}^{\dagger} \lambda_3 \varphi_{\mathbf{k}s}), (\varphi_{\mathbf{k}s}^{\dagger} \lambda_4 \varphi_{\mathbf{k}s}, \varphi_{\mathbf{k}s}^{\dagger} \lambda_6 \varphi_{\mathbf{k}s}), (\varphi_{\mathbf{k}s}^{\dagger} \lambda_5 \varphi_{\mathbf{k}s}, \varphi_{\mathbf{k}s}^{\dagger} \lambda_7 \varphi_{\mathbf{k}s}).
\end{aligned}$$

Since H_0 itself is invariant under any D_{3h} symmetry operation, thereby belongs to A_1' representations, we require that $\xi_{\mathbf{k}}^{\tau}$ belong to different irreducible representations as follows,

$$\begin{aligned}
A_1' &: \xi_{\mathbf{k}}^0, \xi_{\mathbf{k}}^8, \\
A_2' &: \xi_{\mathbf{k}}^2, \\
E' &: (\xi_{\mathbf{k}}^1, \xi_{\mathbf{k}}^3), (\xi_{\mathbf{k}}^4, \xi_{\mathbf{k}}^6), (\xi_{\mathbf{k}}^5, \xi_{\mathbf{k}}^7).
\end{aligned}$$

Considering A_2' representation need longer bonds and $(\xi_{\mathbf{k}}^5, \xi_{\mathbf{k}}^7)$ will break time reversal symmetry in general, we have $\xi_{\mathbf{k}}^2 = \xi_{\mathbf{k}}^5 = \xi_{\mathbf{k}}^7 = 0$. With the help of CG coefficients, we obtain Eq.(4) in the main text.

Fig.S1 shows that the set of tight-binding paramters given in the main text well reproduce the energy dispersion along high symmetry lines and the density of states near the Fermi level.

DERIVE THE THREE-ORBITAL HUBBARD MODEL

The electron field operator $\hat{\psi}_{\sigma}(\vec{r})$ can be expanded in terms of a complete set of Wannier functions,

$$\hat{\psi}_{\sigma}(\vec{r}) = \sum_{m} \sum_{i} w_{im}(\vec{r}) c_{im\sigma},$$

where $c_{im\sigma}$ annihilates an electron with orbital m and spin σ at lattice site i. A generic interacting Hamiltonian is given by

$$H_{int} = \frac{1}{2} \sum_{\sigma\sigma'} \int \hat{\psi}_{\sigma}^{\dagger}(\vec{r}_1) \hat{\psi}_{\sigma'}^{\dagger}(\vec{r}_2) V(\vec{r}_1 - \vec{r}_2) \hat{\psi}_{\sigma'}(\vec{r}_2) \hat{\psi}_{\sigma}(\vec{r}_1) d\vec{r}_1 d\vec{r}_2,$$

where $V_{ext}(\vec{r})$ is external periodic potential, and $V(\vec{r}_1 - \vec{r}_2)$ is the screened Coulomb interaction. H_0 can be written as a tight-binding model and we shall focus on the interacting part H_{int}. In the spirit of a Hubbard type approximation, i.e. retaining only the terms on the same lattice site, we have

$$H_{int} = \frac{1}{2} \sum_{i} \sum_{mnm'n'} \sum_{\sigma\sigma'} V_{mm',n'n} c_{im\sigma}^{\dagger} c_{im'\sigma'}^{\dagger} c_{in'\sigma'} c_{in\sigma},$$

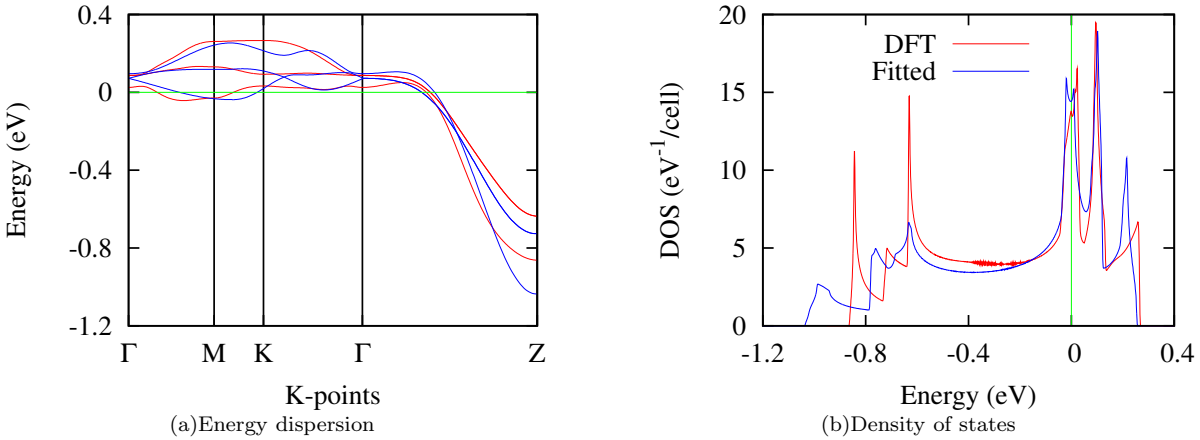

(a)Energy dispersion (b)Density of states

FIG. S1: Comparison of the energy dispersion along high symmetry lines (a) and the density of states (b) for $K_2Cr_3As_3$ obtained from the DFT calculation and from the present model Hamiltonian. The red and blue lines are the results obtained with DFT calculation and the model calculation, respectively.

where

$$V_{mm',n'n} = \int w^*_{im}(\vec{r}_1)w^*_{im'}(\vec{r}_2)V(\vec{r}_1-\vec{r}_2)w_{in'}(\vec{r}_2)w_{in}(\vec{r}_1)d\vec{r}_1d\vec{r}_2.$$

Let's consider nonvanishing $V_{mm',n'n}$ according to D_{3h} group symmetry. Since the interaction $V(\vec{r}_1-\vec{r}_2) = V(|\vec{r}_1-\vec{r}_2|)$ respects the full point group symmetry and belong to the A_1 representation. Wether a $V_{mm',n'n}$ vanishes can be determined by the CG coefficients.

Firstly, for $m, n = 1, 2$, the nonzero $V_{mm',n'n}$ can be written in terms of the integrals explicitly,

$$\begin{aligned}
V_{mm,mm} &= \int |w_{im}(\vec{r}_1)|^2V(\vec{r}_1-\vec{r}_2)|w_{im}(\vec{r}_2)|^2d\vec{r}_1d\vec{r}_2 = U_1,\\
V_{m\bar{m},\bar{m}m} &= \int |w_{im}(\vec{r}_1)|^2V(\vec{r}_1-\vec{r}_2)|w_{i\bar{m}}(\vec{r}_2)|^2d\vec{r}_1d\vec{r}_2 = U_2,\\
V_{m\bar{m},m\bar{m}} &= \int w^*_{im}(\vec{r}_1)w_{i\bar{m}}(\vec{r}_1)V(\vec{r}_1-\vec{r}_2)w^*_{i\bar{m}}(\vec{r}_2)w_{im}(\vec{r}_2)d\vec{r}_1d\vec{r}_2 = J,\\
V_{mm,\bar{m}\bar{m}} &= \int w^*_{im}(\vec{r}_1)w_{i\bar{m}}(\vec{r}_1)V(\vec{r}_1-\vec{r}_2)w_{i\bar{m}}(\vec{r}_2)w^*_{im}(\vec{r}_2)d\vec{r}_1d\vec{r}_2 = J^*.
\end{aligned}$$

where U_1 is the intra-orbital interaction and U_2 is the inter-orbital interaction. If one chooses the Wannier function to be real, then $J^* = J$, and J is the Hund's exchange energy.

Secondly, we can choose that $|1\rangle$ transfers as x and $|2\rangle$ transfers as y under D_{3h} symmetry operations. Note that $V(\vec{r}_1-\vec{r}_2)$ is invariant not only under D_{3h} symmetry operations, but also under all the $O(3)$ symmetry operations. So that $V_{xx,xx} = V_{yy,yy} = U_1$. Under a C_3 rotation along the c-axis, the two Wannier functions $|1\rangle$ and $|2\rangle$ (denoted by x and y) transfer as

$$\begin{aligned}
w_x &\rightarrow \cos\theta w_x + \sin\theta w_y,\\
w_y &\rightarrow -\sin\theta w_x + \cos\theta w_y,
\end{aligned}$$

where $\theta = \frac{2\pi}{3}$. The integral $V_{xx,xx}$ should keep invariant under this operation. Assuming w_x and w_y are real, after straightforward algebra, we have

$$U_1 = (\cos^4\theta + \sin^4\theta)U_1 + 2U_2\cos^2\theta\sin^2\theta + 4\cos^2\theta\sin^2\theta J,$$

where the transfermation peroperties under C_2 are used. From the above, we have

$$U_1 = U_2 + 2J.$$

Thirdly, we involve the state $|3\rangle$. For $m, m' = 1, 2$ (or x, y), the relevant nonvanishing terms are given in the following,

$$\begin{aligned}
V_{33,33} &= \int |w_{i3}(\vec{r}_1)|^2 V(\vec{r}_1 - \vec{r}_2)|w_{i3}(\vec{r}_2)|^2 d\vec{r}_1 d\vec{r}_2 = U_1', \\
V_{3m,m3} &= \int |w_{im}(\vec{r}_1)|^2 V(\vec{r}_1 - \vec{r}_2)|w_{i3}(\vec{r}_2)|^2 d\vec{r}_1 d\vec{r}_2 = U_2', \\
V_{m3,m3} &= \int w_{im}^*(\vec{r}_1) w_{i3}(\vec{r}_1) V(\vec{r}_1 - \vec{r}_2) w_{i3}^*(\vec{r}_2) w_{im}(\vec{r}_2) d\vec{r}_1 d\vec{r}_2 = J', \\
V_{mm',33} &= \int w_{im}^*(\vec{r}_1) w_{i3}(\vec{r}_1) V(\vec{r}_1 - \vec{r}_2) w_{im'}^*(\vec{r}_2) w_{i3}(\vec{r}_2) d\vec{r}_1 d\vec{r}_2 = J''_{mm'}.
\end{aligned}$$

When Wannier functions are real, $J''_{mm} = J'$. For $m \neq m'$, we set $m = x$ and $m' = y$, thus under the C_3 rotation,

$$J''_{xx} = \cos^2\theta J''_{xx} + \sin^2\theta J''_{yy} + 2\cos\theta\sin\theta J''_{xy} = J''_{xx} + 2\cos\theta\sin\theta J''_{xy}.$$

The above gives rise to

$$J''_{xy} = 0.$$

In summary, we have

$$\begin{aligned}
H_{int} &= \frac{1}{2}\sum_{i,\sigma\sigma'}\Bigg\{\sum_{m=1}^{2}(U_1 c_{im\sigma}^\dagger c_{im\sigma'}^\dagger c_{im\sigma'} c_{im\sigma} + U_2 c_{im\sigma}^\dagger c_{i\bar{m}\sigma'}^\dagger c_{i\bar{m}\sigma'} c_{im\sigma} + J c_{im\sigma}^\dagger c_{i\bar{m}\sigma'}^\dagger c_{im\sigma'} c_{i\bar{m}\sigma} + J c_{im\sigma}^\dagger c_{im\sigma'}^\dagger c_{i\bar{m}\sigma'} c_{i\bar{m}\sigma}) \\
&\quad + U_1' c_{i3\sigma}^\dagger c_{i3\sigma'}^\dagger c_{i3\sigma'} c_{i3\sigma} + \sum_m [U_2' c_{im\sigma}^\dagger c_{is3\sigma'}^\dagger c_{is3\sigma'} c_{im\sigma} + J' c_{im\sigma}^\dagger c_{i3\sigma'}^\dagger c_{im\sigma'} c_{i3\sigma} + J'(c_{im\sigma}^\dagger c_{im\sigma'}^\dagger c_{i3\sigma'} c_{i3\sigma} + h.c.)]\Bigg\} \\
&= \frac{1}{2}\sum_{i,\sigma}\sum_{m=1}^{2}[U_1 c_{im\sigma}^\dagger c_{im\bar{\sigma}}^\dagger c_{im\bar{\sigma}} c_{im\sigma} + J c_{im\sigma}^\dagger c_{im\bar{\sigma}}^\dagger c_{i\bar{m}\bar{\sigma}} c_{i\bar{m}\sigma} + J'(c_{im\sigma}^\dagger c_{im\bar{\sigma}}^\dagger c_{i3\bar{\sigma}} c_{i3\sigma} + h.c.)] \\
&\quad + \frac{1}{2}\sum_{i,\sigma\sigma'}\sum_{m=1}^{2}(U_2 c_{im\sigma}^\dagger c_{i\bar{m}\sigma'}^\dagger c_{i\bar{m}\sigma'} c_{im\sigma} + J c_{im\sigma}^\dagger c_{i\bar{m}\sigma'}^\dagger c_{im\sigma'} c_{i\bar{m}\sigma} + U_2' c_{im\sigma}^\dagger c_{i3\sigma'}^\dagger c_{i3\sigma'} c_{im\sigma} + J' c_{im\sigma}^\dagger c_{i3s\sigma'}^\dagger c_{im\sigma'} c_{i3\sigma}) \\
&\quad + \frac{1}{2}\sum_{i,\sigma} U_1' c_{i3\sigma}^\dagger c_{i3\bar{\sigma}}^\dagger c_{i3\bar{\sigma}} c_{i3\sigma},
\end{aligned}$$

where $\bar{m}$ is the opposite orbital to m within the E representation, and $\bar{\sigma}$ is the opposite spin to σ.

RPA FOR EFFECTIVE PAIRING INTERACTION

We shall generalized the calculation by Scalapino et al. to the multi-orbital case. Diagramatically, RPA contains two types Feynman diagrams beside the bare vertex function $V_0(\mathbf{k}, \mathbf{k}')$ as shown in Fig. S2. One contains the bubble diagrams, the other contains the ladder diagrams with Cooperon.

For the single orbital case, the RPA effective pairing interaction for spin-singlet and spin-triplet channels are

$$\begin{aligned}
V_s(\mathbf{k}, \mathbf{k}') &= \frac{U}{1 - U^2\chi_0^2(\mathbf{k} - \mathbf{k}')} + \frac{U^2\chi_0(\mathbf{k} + \mathbf{k}')}{1 - U\chi_0(\mathbf{k} + \mathbf{k}')}, \\
V_t(\mathbf{k}, \mathbf{k}') &= -\frac{U^2\chi_0(\mathbf{k} - \mathbf{k}')}{1 - U^2\chi_0^2(\mathbf{k} - \mathbf{k}')}.
\end{aligned}$$

Note that Fig. S2(c) is absent in U_s and Fig. S2(b), (d), (e) and (f) are absent in V_t because $\sigma' = \bar{\sigma}$ in the U term.

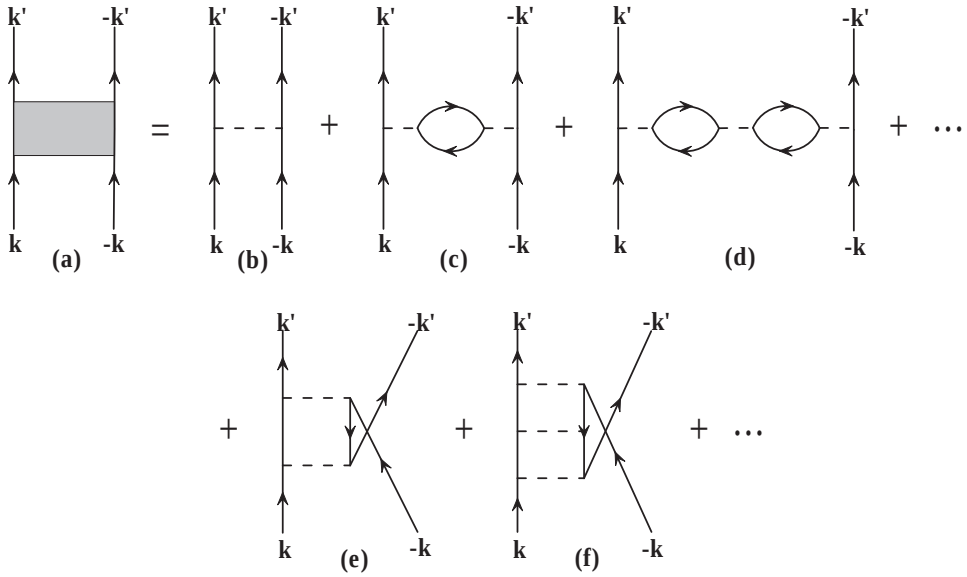

FIG. S2: Feynman diagram for RPA calculation of effective pairing interaction $V(\mathbf{k},\mathbf{k}')$. (a) Effective vertex function $V(\mathbf{k},\mathbf{k}')$. (b) Bare vertex function $V_0(\mathbf{k},\mathbf{k}')$. (c) and (d) Bubble diagrams. (e) and (f) Ladder digarams with Cooperon.

For multi-obtial case, we shall replace the numbers U and χ_0 by the bare vertex functions $\hat{\Gamma}_{s(t)}$ in Eq. (9) and susceptibility tensor $\hat{\chi}_0$ in Eq. (5) in the main text. The effective pairing interaction $\hat{V}_{s(t)}(\mathbf{k},\mathbf{k}')$ from the bubble diagrams are

$$\begin{aligned}\hat{V}_s^{bub}(\mathbf{k},\mathbf{k}') &= \hat{\Gamma}_s - \hat{\Gamma}_s\hat{\chi}_0(\mathbf{q})\hat{\Gamma}_t - \hat{\Gamma}_t\hat{\chi}_0(\mathbf{q})\hat{\Gamma}_s \\ &\quad +\hat{\Gamma}_s\hat{\chi}_0(\mathbf{q})\hat{\Gamma}_t\hat{\chi}_0(\mathbf{q})\hat{\Gamma}_t + \hat{\Gamma}_t\hat{\chi}_0(\mathbf{q})\hat{\Gamma}_s\hat{\chi}_0(\mathbf{q})\hat{\Gamma}_t + \hat{\Gamma}_t\hat{\chi}_0(\mathbf{q})\hat{\Gamma}_t\hat{\chi}_0(\mathbf{q})\hat{\Gamma}_s + \hat{\Gamma}_s\hat{\chi}_0(\mathbf{q})\hat{\Gamma}_s\hat{\chi}_0(\mathbf{q})\hat{\Gamma}_s + \cdots \\ &\quad +\hat{\Gamma}_s\hat{\chi}_0(\mathbf{p})\hat{\Gamma}_s + \hat{\Gamma}_s\hat{\chi}_0(\mathbf{p})\hat{\Gamma}_s\hat{\chi}_0(\mathbf{p})\hat{\Gamma}_s + \cdots \\ &= \frac{1}{2}(\hat{\Gamma}_t+\hat{\Gamma}_s)[1+\hat{\chi}_0(\mathbf{q})(\hat{\Gamma}_t+\hat{\Gamma}_s)]^{-1} - \frac{1}{2}(\hat{\Gamma}_t-\hat{\Gamma}_s)[1+\hat{\chi}_0(\mathbf{q})(\hat{\Gamma}_t-\hat{\Gamma}_s)]^{-1}\end{aligned}$$

and

$$\begin{aligned}\hat{V}_t^{bub}(\mathbf{k},\mathbf{k}') &= \hat{\Gamma}_t - \hat{\Gamma}_s\hat{\chi}_0(\mathbf{q})\hat{\Gamma}_s - \hat{\Gamma}_t\hat{\chi}_0(\mathbf{q})\hat{\Gamma}_t \\ &\quad +\hat{\Gamma}_t\hat{\chi}_0(\mathbf{q})\hat{\Gamma}_t\hat{\chi}_0(\mathbf{q})\hat{\Gamma}_t + \hat{\Gamma}_t\hat{\chi}_0(\mathbf{q})\hat{\Gamma}_s\hat{\chi}_0(\mathbf{q})\hat{\Gamma}_s + \hat{\Gamma}_s\hat{\chi}_0(\mathbf{q})\hat{\Gamma}_t\hat{\chi}_0(\mathbf{q})\hat{\Gamma}_s + \hat{\Gamma}_s\hat{\chi}_0(\mathbf{q})\hat{\Gamma}_s\hat{\chi}_0(\mathbf{q})\hat{\Gamma}_t + \cdots \\ &\quad +\hat{\Gamma}_t\hat{\chi}_0(\mathbf{p})\hat{\Gamma}_t + \hat{\Gamma}_t\hat{\chi}_0(\mathbf{p})\hat{\Gamma}_t\hat{\chi}_0(\mathbf{p})\hat{\Gamma}_t + \cdots \\ &= \frac{1}{2}(\hat{\Gamma}_t+\hat{\Gamma}_s)[1+\hat{\chi}_0(\mathbf{q})(\hat{\Gamma}_t+\hat{\Gamma}_s)]^{-1} + \frac{1}{2}(\hat{\Gamma}_t-\hat{\Gamma}_s)[1+\hat{\chi}_0(\mathbf{q})(\hat{\Gamma}_t-\hat{\Gamma}_s)]^{-1},\end{aligned}$$

while those from ladder diagrams are

$$\begin{aligned}\check{V}_s^{lad}(\mathbf{k},\mathbf{k}') &= \check{\Gamma}_s\hat{\chi}_0(\mathbf{p})\check{\Gamma}_s + \check{\Gamma}_s\hat{\chi}_0(\mathbf{p})\check{\Gamma}_s\hat{\chi}_0(\mathbf{p})\check{\Gamma}_s + \cdots \\ &= \check{\Gamma}_s\hat{\chi}_0(\mathbf{p})\check{\Gamma}_s[1-\hat{\chi}_0(\mathbf{p})\check{\Gamma}_s]^{-1}\end{aligned}$$

and

$$\begin{aligned}\check{V}_t^{lad}(\mathbf{k},\mathbf{k}') &= \check{\Gamma}_t\hat{\chi}_0(\mathbf{p})\check{\Gamma}_t + \check{\Gamma}_t\hat{\chi}_0(\mathbf{p})\check{\Gamma}_t\hat{\chi}_0(\mathbf{p})\check{\Gamma}_t + \cdots \\ &= \check{\Gamma}_t\hat{\chi}_0(\mathbf{p})\check{\Gamma}_t[1-\hat{\chi}_0(\mathbf{p})\check{\Gamma}_t]^{-1},\end{aligned}$$

where $\mathbf{p}=\mathbf{k}+\mathbf{k}'$ and $\mathbf{q}=\mathbf{k}-\mathbf{k}'$, and the matrix $\check{A}$ is related to matrix $\hat{A}$ through the following relation,

$$\check{A}_{mn,m'n'} = \hat{A}_{nn',m'm}.$$

Matrix summation in the bubble diagrams

Below we write down the details on summing over the two series of matrice in the bubble diagrams,

$$\begin{aligned}\hat{A} &= \hat{\Gamma}_s - \hat{\Gamma}_s\hat{\chi}_0(\mathbf{q})\hat{\Gamma}_t - \hat{\Gamma}_t\hat{\chi}_0(\mathbf{q})\hat{\Gamma}_s \\ &\quad +\hat{\Gamma}_s\hat{\chi}_0(\mathbf{q})\hat{\Gamma}_t\hat{\chi}_0(\mathbf{q})\hat{\Gamma}_t + \hat{\Gamma}_t\hat{\chi}_0(\mathbf{q})\hat{\Gamma}_s\hat{\chi}_0(\mathbf{q})\hat{\Gamma}_t + \hat{\Gamma}_t\hat{\chi}_0(\mathbf{q})\hat{\Gamma}_t\hat{\chi}_0(\mathbf{q})\hat{\Gamma}_s + \hat{\Gamma}_s\hat{\chi}_0(\mathbf{q})\hat{\Gamma}_s\hat{\chi}_0(\mathbf{q})\hat{\Gamma}_s + \cdots\end{aligned}$$

and

$$\begin{aligned}\hat{B} &= \hat{\Gamma}_t - \hat{\Gamma}_s\hat{\chi}_0(\mathbf{q})\hat{\Gamma}_s - \hat{\Gamma}_t\hat{\chi}_0(\mathbf{q})\hat{\Gamma}_t \\ &\quad +\hat{\Gamma}_t\hat{\chi}_0(\mathbf{q})\hat{\Gamma}_t\hat{\chi}_0(\mathbf{q})\hat{\Gamma}_t + \hat{\Gamma}_t\hat{\chi}_0(\mathbf{q})\hat{\Gamma}_s\hat{\chi}_0(\mathbf{q})\hat{\Gamma}_s + \hat{\Gamma}_s\hat{\chi}_0(\mathbf{q})\hat{\Gamma}_t\hat{\chi}_0(\mathbf{q})\hat{\Gamma}_s + \hat{\Gamma}_s\hat{\chi}_0(\mathbf{q})\hat{\Gamma}_s\hat{\chi}_0(\mathbf{q})\hat{\Gamma}_t + \cdots\end{aligned}$$

where every term in $\hat{A}$ cotains odd number of $\hat{\Gamma}_s$ and every term in $\hat{B}$ contains even number of $\hat{\Gamma}_s$, and each $\hat{\chi}_0$ contribute one minus sign. To do this summation, we multiple $\hat{\chi}_0(\mathbf{q})$ at both sides at first, then add them together or substract one to another. Hence

$$\begin{aligned}\hat{\chi}_0(\mathbf{q})\hat{B} + \hat{\chi}_0(\mathbf{q})\hat{A} &= \hat{\chi}_0(\mathbf{q})(\hat{\Gamma}_t + \hat{\Gamma}_s)[1 + \hat{\chi}_0(\mathbf{q})(\hat{\Gamma}_t + \hat{\Gamma}_s)]^{-1}, \\ \hat{\chi}_0(\mathbf{q})\hat{B} - \hat{\chi}_0(\mathbf{q})\hat{A} &= \hat{\chi}_0(\mathbf{q})(\hat{\Gamma}_t - \hat{\Gamma}_s)[1 + \hat{\chi}_0(\mathbf{q})(\hat{\Gamma}_t - \hat{\Gamma}_s)]^{-1}.\end{aligned}$$

Then we obtain that

$$\begin{aligned}\hat{A} &= \frac{1}{2}(\hat{\Gamma}_t + \hat{\Gamma}_s)[1 + \hat{\chi}_0(\mathbf{q})(\hat{\Gamma}_t + \hat{\Gamma}_s)]^{-1} - \frac{1}{2}(\hat{\Gamma}_t - \hat{\Gamma}_s)[1 + \hat{\chi}_0(\mathbf{q})(\hat{\Gamma}_t - \hat{\Gamma}_s)]^{-1}, \\ \hat{B} &= \frac{1}{2}(\hat{\Gamma}_t + \hat{\Gamma}_s)[1 + \hat{\chi}_0(\mathbf{q})(\hat{\Gamma}_t + \hat{\Gamma}_s)]^{-1} + \frac{1}{2}(\hat{\Gamma}_t - \hat{\Gamma}_s)[1 + \hat{\chi}_0(\mathbf{q})(\hat{\Gamma}_t - \hat{\Gamma}_s)]^{-1}.\end{aligned}$$

INTEGRATION OVER THE FERMI SURFACE

To calculate the dimensionless coupling constant Λ, we need to integrate over the Fermi surface. However, it is difficult to do this kind integration numerically. Insteadly, we recall the method to calculation DOS. The DOS is derived as follows,

$$D(\epsilon) = \int_{S(\epsilon)} \frac{dS_{\mathbf{k}}}{(2\pi)^3}\frac{\delta k(\mathbf{k})}{d\epsilon} = \int \frac{dS_{\mathbf{k}}}{(2\pi)^3}\frac{1}{|\mathbf{v}_{\mathbf{k}}|}.$$

Numerically, we use the following Lorentz lineshape to calculate it,

$$D(\epsilon) = \frac{1}{\pi N}\sum_{\mathbf{k}} \frac{\delta}{(\epsilon_{\mathbf{k}} - \epsilon)^2 + \delta^2},$$

where N is the number of k-points in the first Brillouin zone and δ is the width of Lorentz lineshape. Thus, the integration in Λ can be converted to

$$\Lambda = -\frac{\delta\sum_{\mathbf{k},\mathbf{k}'}\frac{1}{(\epsilon_{\mathbf{k}}-\mu)^2+\delta^2}\frac{1}{(\epsilon_{\mathbf{k}'}-\mu)^2+\delta^2}g^*(\mathbf{k})V(\mathbf{k},\mathbf{k}')g(\mathbf{k}')}{\pi N\sum_{\mathbf{k}}\frac{1}{(\epsilon_{\mathbf{k}}-\mu)^2+\delta^2}|g(\mathbf{k})|^2}.$$